ELSEVIER

Chemical Geology 200 (2003) 1–24

CHEMICAL GEOLOGY
INCLUDING
ISOTOPE GEOSCIENCE

www.elsevier.com/locate/chemgeo

Relationship between submarine MORB glass textures and atmospheric component of MORBs

Hidenori Kumagai *,[1], Ichiro Kaneoka

Earthquake Research Institute, The University of Tokyo, Bunkyo-ku, Tokyo 113-0032, Japan

Received 9 January 2002; accepted 21 February 2003

Abstract

We investigated the relationship between noble gas signatures and sample textures among glassy fragments. Glassy MORB fragments were classified based on their texture. By handpicking under a binocular, they were divided into three groups: (1) heterogeneous ''outer'' part, (2) homogeneous ''middle'' part, and (3) ''inner'' neighbors of the transition zone. Their noble gas signatures were analyzed by the step heating method. The state of homogeneities of the samples identified under a microscope was confirmed semi-quantitatively by measuring refractive indices of the fragments. The ''outer'' heterogeneous part characterized by devitrified and/or color changed regions was significantly affected by the atmospheric component as indicated by the relatively large amount of gases released with almost atmospheric $^{40}Ar/^{36}Ar$ and $^{20}Ne/^{22}Ne$ in the 400 °C fraction. The transition ''inner'' part of glassy rind adjacent to the crystallized interior which is characterized by the appearance of quenched microcrystals has lost the magma-derived component and is contaminated by some kinetic processes: it showed a small amount of noble gases except for Ne with a low $^{20}Ne/^{22}Ne$ ratio. The homogeneous ''middle'' part turns out to be least affected by contamination and is regarded to mostly retain magma-derived noble gas signatures. It is characterized by the most abundant He and the highest $^{40}Ar/^{36}Ar$ as a total ratio with similar values in both the middle and the high temperature fractions. This part is also characterized by lower refractive index values and a small deviation compared to the nonhomogeneous parts. Hence, for noble gas analyses of MORB glasses, it is recommended to select homogeneous ''clear'' glasses by excluding color changed and/or devitrified weathering part and quenched microcrystals.

Keywords: Noble gas; Atmospheric component; MORB glass; Texture of glass matrix; Refractive index

1. Introduction

Recently, extensive noble gas studies have focused on the atmosphere-like component in the mantle, which is frequently interpreted as recycling atmospheric component by subducting slabs (e.g. Bach and Niedermann, 1998; Sarda et al., 1999; Matsumoto et al., 2001). These studies implicitly have assumed that the observed atmospheric component, which was

* Corresponding author. Deep Sea Res. Department, Japan Marine Science and Technology Center (JAMSTEC), Yokosuka, Kanagawa 237-0061, Japan. Tel.: +81-46-867-9333; fax: +81-46-867-9315.

E-mail address: kumagai@jamstec.go.jp (H. Kumagai).

[1] From November 2002 to October 2003: c/o Dr. Henry Dick, MS#8, Woods Hole Oceanographic Institution, 266 Woods Hole Road, Woods Hole, MA 02543, USA.

0009-2541/03/$ - see front matter © 2003 Elsevier B.V. All rights reserved.
doi:10.1016/S0009-2541(03)00077-9

derived from the secondary effect of alteration and/or weathering of samples, was excluded by experimental and analytical techniques. However, Ballentine and Barfod (2000) have pointed out that significant parts of the observed atmospheric components represent non-fractionated abundances. They have argued that such atmospheric components were derived from laboratory handling based on the relationship between ^{22}Ne normalized elemental abundance patterns and ^{20}Ne/^{22}Ne ratios.

Many efforts have been made to reduce the effect of atmospheric contamination in noble gas signatures in order to obtain the intrinsic signatures of various types of magmas and their sources. For example, the stepwise-crushing gas extraction method was applied to one of the most gas-rich MORB samples, 2ΠD43, the so-called "popping rock" (Moreira et al., 1998). Although more than 1 g was used, it still shows a sign of atmospheric contamination for each isotope in each crushing step: ^{40}Ar/^{36}Ar ranges from 1000 to 25,000. Burnard et al. (1997) applied the laser extraction technique to aliquots of the same sample 2ΠD43. Although a laser probe makes it possible to analyze the ^{40}Ar/^{36}Ar in a single bubble, large variations in the ratio have been recorded, ranging from 3600 up to 42,000 for the ratio. Based on such observations, they suggested that all observed ^{36}Ar were derived from atmospheric contamination and magma should contain only ^{40}Ar originally. Both experiments imply that the degree of atmospheric contamination might be variable even in a single sample.

Contrarily, if we apply careful sample selection, there is a possibility to reduce the atmospheric contamination because contamination level might be related to the heterogeneity of the sample caused by weathering and/or alteration (Kumagai, 1999). Although chilled glassy rims are usually used for noble gas analyses of MORBs, contacting with seawater during and after solidification directly cools the surface portion, and seawater might affect the glassy rim at least partly. A submarine-erupted glassy fragment with a low vesicularity of much less than 1% usually has large textural heterogeneities on the millimeter scale and shows rather heterogeneous distribution of vesicles, which has been revealed by a trial about the detailed noble gas signatures within glasses of a single basaltic pillow (e.g. Hiyagon, 1992; Kumagai and Kaneoka, 1998).

We have shown that, in order to reduce the amount of atmospheric components, the middle portion of a thick glassy rind of a submarine pillow should be separated both from the surface glass and the inner part mixed with quenched crystals (Kumagai and Kaneoka, 1998). However, the original surface of a pillow rarely remains intact because glassy rinds are easily detached and broken in many cases.

In this study, we examined the relationship between sample textures and noble gas signatures with the following intentions: (1) the atmospheric component of the sample might be reduced by careful sample selection, and (2) the textures of glass matrices might reflect on the kinds of contained components. The results of the study contribute to establishing a sample treatment scheme to reduce the secondary effect for noble gas signatures especially for MORB glasses. If we could exclude during- and post-eruption contamination by the atmospheric component, ^{40}Ar/^{36}Ar can be used as a sensitive tracer to reveal magmatic processes, such as the mixing process between different batches of magmas and interactions with surface materials in hydrothermal systems.

In order to evaluate the relationship between noble gas signatures and sample textures among glassy fragments, we focused on the variation of ^{40}Ar/^{36}Ar, because Ar is more abundant in seawater than the other noble gases and the effect of alteration and/or weathering occurring in seawater could be most easily monitored by ^{40}Ar/^{36}Ar. Furthermore, to evaluate the condition of glassy samples, refractive indices were examined for present samples because the refractive index has been regarded to be sensitive to the physicochemical condition of glassy materials (e.g. Steen-McIntyre, 1975).

2. Samples

Samples used in this study are fragments of chilled glassy margins of tholeiitic basalts recovered from depths ranging from 3600 to 4100 m by dredging (KH93-3 Cruise, ORI, The University of Tokyo, 1993; Fujii et al., 1995).

Plate 1 shows an example of a secondary electron image (SEI) for a typical fragment of sample DR6A1 taken by the scanning electron microscope (SEM). In

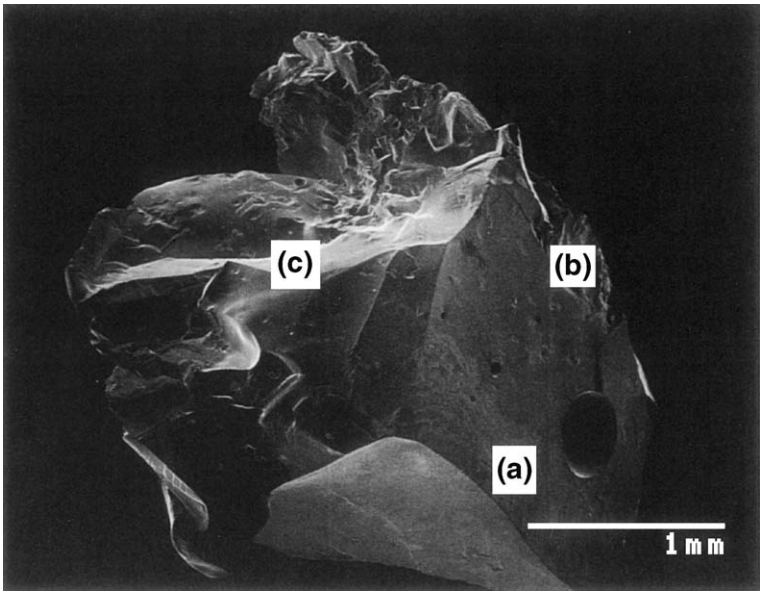

Plate 1. Secondary electron image (SEI) of a fragment of sample DR6A1 taken by scanning electron microscope (SEM; Hitachi S-530, ERI). (a) A region of "rough" surface. (b) A region which contains relatively abundant phenocrysts. (c) Almost aphyric homogeneous glass.

this plate, at least three regions with different characteristics can be recognized within a single glassy chip of 3 mm in size: regions represented by (a) a "rough" surface, (b) a phase with relatively abundant phenocrysts, and (c) almost aphyric homogeneous glass, respectively. Plagioclases are the most abundant phenocrysts up to 1 mm in size and sparse olivines are observed in the thin section. It also shows a quite low vesicularity (much lower than 1%). The sizes of vesicles are typically smaller than 100 μm in diameter. However, much larger vesicles are observed occasionally with the maximum of 300 μm in this fragment (just above the scale bar).

Plate 2 is a magnified SEM image for a rough surface area. In the SEI (upper plate), the occasional distribution of amorphous adherents up to 5 μm in size indicates that the original surface had been exposed to seawater. Abundant small pores are scattered in the broken surfaces occasionally linked to one another. In the back-scattered electron image (BEI, lower plate), such pores are surrounded by a dark region, which implies that the region has a relatively small average molar weight. Although this dark region is localized with a typical width of less than 10 μm from the boundary, it extends along the pores more than 20 μm into the bright region. This feature suggests either hydration or removal of heavy elements during alteration and/or weathering along pores. Since the roughness and/or thinness of the region prevented the samples from the accurate chemical measurement, only qualitative EDS-XRF measurement was applied. Observed quite small Na-peaks compared to those of normal glass region suggest dissolution of alkaline elements into seawater. Then a refractive index analysis was performed to evaluate the degree of hydration for present samples.

2.1. Preparation of samples for noble gas analysis

In this study, two or three groups separated from individual pillow fragments were compared in each experiment (Table 1).

Series 1: samples were prepared from the single pillow fragment DR3A1 (see Appendix A; Fujii et al., 1995). In order to clarify the relationship between noble gas signatures and optically observed textures of samples, the fragments were divided into three groups using the following criteria (Plate 3). (1) Group "outer": this group is usually related to either

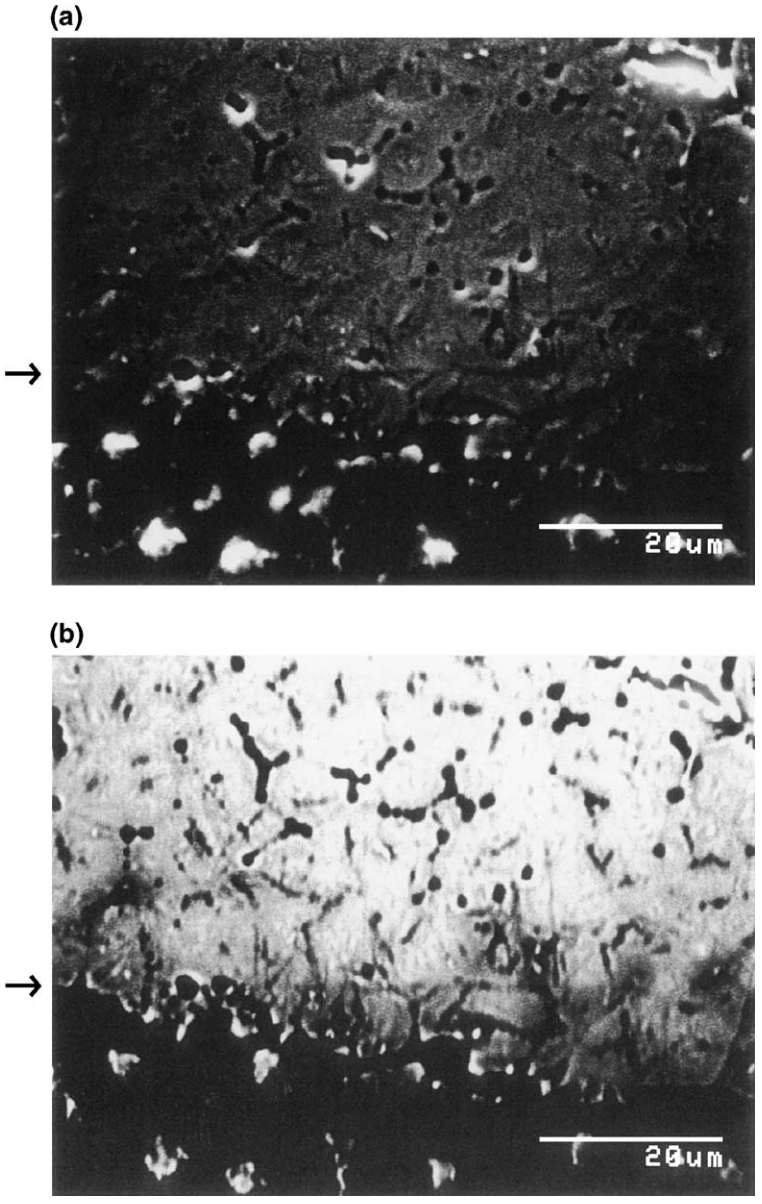

Plate 2. SEM images of a fragment which corresponds to the group "usual" in Series 2 experiment. (a) SEI. (b) Back-scattered electron image (BEI). Based on the interpretation of abundant adherents, the lower parts of both images are regarded as the original surfaces exposed to seawater. The upper parts are newly broken surfaces generated during sample preparation. Assumed boundaries are shown by arrows: located at one-thirds from the bottom of the plate.

the outermost margin of glassy rinds or parts adjacent to cracks. They show an apparent sign of heterogeneity: a rough, not smooth surface after ultrasonic cleaning with diluted HNO_3, and/or devitrified areas, and/or remaining adherents, and/or interference color. Such heterogeneities were usually localized in a rather thin layer, which is easily identified by the lack of the adjacent section of the broken surface (Plate 3a). (2) Group "middle": this group is quite clear, homogeneous glass regarded as a middle position in the rinds

Table 1
Sample preparation procedure and experimental conditions

Series No. of experiment	Description	Chip size	HNO_3 treatment	Extraction
Series 1: Comparison within single sample rock				
Outer	outermost margin or parts of adjacent to cracks in glassy rind	<1 mm	done	heating
Middle	middle position of glassy rind, between outer and inner group	<1 mm	done	heating
Inner	near the transition zone to a crystallized interior	<1 mm	done	heating
Series 2: Comparison "clear" samples with "usual" ones				
Usual	roughly characterized as glass-rich parts, excluding apparent crystalline zone	several millimeters	none	heating
Clear	neither containing quench crystals nor showing any signs of heterogeneities under binocular	<1 mm	done	heating
Series 3: Comparison crushing with heating extraction				
Crushing	roughly characterized as glass-rich parts	>several millimeters	none	crushing
Heating	cut from thick glassy layer (or "clear" group)	~ several millimeters	done	heating

of pillow between those of the groups "outer" and "inner". (3) Group "inner": this group is regarded as near the transition zone to a crystallized interior of the pillow. Chips in this group are characterized by containing over-growth microcrystals around phenocrysts (see magnified SEM photograph, Plate 4), which is recognized as haloes around phenocrysts and/or spherules as spots within glassy matrices using a binocular with magnification of a few tens. This feature suggests that the cooling rate of this group is relatively low compared with the other groups. Fig. 1a shows schematically an example of positions and relation.

Glassy fragments with several millimeters in size were separated on board and crushed to less than one millimeter in size for selection. Through the process of selection, plagioclase phenocrysts exceeding ca. 0.5 mm in size were excluded. Vesicles of smaller than a half millimeter in diameter were rarely observed during this process. Separating yields of each group in the present sample which is regarded to be a typical macroscopically glass-rich fragment are roughly 50%, 30% and 20% for the groups "outer", "middle" and "inner", respectively. An amount of ca. 1 g for each group was used for analyses.

Series 2: two sets of samples were prepared to compare with the result of Series 1. Samples were selected from glassy aliquots separated from two moderately evolved tholeiitic basalts (DR1A1 and DR6A1; details are described in Appendix A). Some glassy chips originally had brownish rust on their surface, most likely a sign of direct contact with seawater. Both samples were divided into two groups. Based on macroscopic observation, fragments roughly characterized as glass-rich parts excluding apparent crystalline zone were labeled as "usual" group.

In order to select "clear" groups, fragments of "usual" groups were further crushed into the size smaller than 1 mm. Ones neither containing quench crystals nor showing any signs of heterogeneities were handpicked. Picking yields are usually less than 30% in weight of the processed "usual" fragments. This proportion is comparable to that of the group "middle" of the Series 1. Fragments of ca. 200 mg and 1 g were weighed as "usual" and "clear" groups, respectively.

Series 3: three samples were prepared for crushing gas-extraction in order to compare with heating extraction: one is sample DR6A1 measured in Series 2.

Others are split from different sample DR25A1 already analyzed by step heating (Kumagai and Kaneoka, 1998). Hereafter, the data reported in Kumagai and Kaneoka (1998) will be referred to

(a)

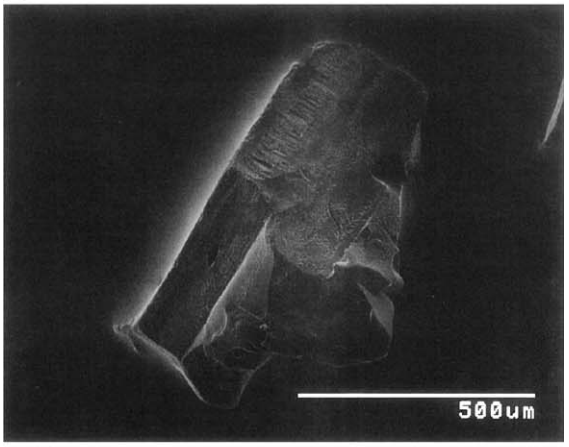

(b)

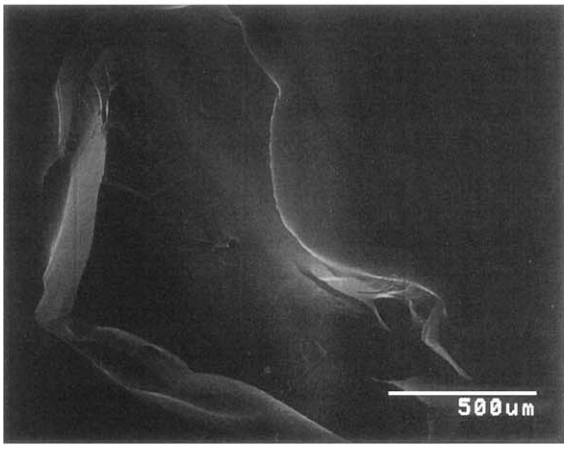

(c)

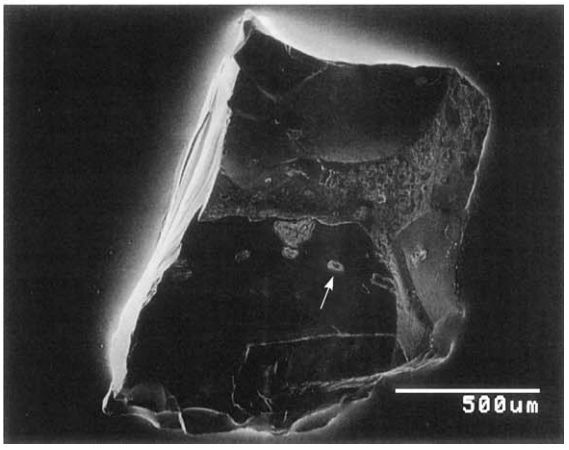

using suffix "b". In the present study, split aliquots from positions b#1 and b#2 of the sample were measured (Fig. 1 of Kumagai and Kaneoka, 1998). These two positions have no quenched crystals: #1 is regarded to contain the part of "outer" group due to the outermost layer of the pillow, but #2 corresponds to the "middle" group located inside of #1. To check the reproducibility of previous heating extraction, two more samples were cut and labeled c#1 and c#2, respectively. Sample c#1 is a 3-mm-thick aliquot from the outermost margin, which corresponds to b#1. Sample c#2 was taken from the inner layer of c#1 and 4 mm thick. It corresponds to the mixture of b#2 and #3. For precise Ne isotope analysis, an aliquot weighing ca. 0.4 g (c#2-2) was further separated. Optical and electron microscope observations have indicated that vesicularities are much lower compared to the Series 2 samples. Typical vesicle size is a few tens micrometers in diameter, and larger vesicles up to 100 μm in diameter were sometimes observed.

Selected fragments were ultrasonically cleaned with diluted HNO_3, distilled water, acetone and ethanol in most cases. The "usual" groups of Series 2 were crushed into chips with several millimeters in size and cleaned with acetone and distilled water. After desiccation at 60 °C for more than 2 h, the weighed samples were wrapped in Al-foil and loaded in the Pyrex glass sample holder for heating extraction. In the Series 3 experiment, samples with several millimeters in size were loaded in a press-type crusher (Hanyu et al., 1999).

2.2. Sample preparation for refractive index measurements

After the Series 2 experiments, refractive indices in different portions within the sample DR6A1 were examined in order to estimate its optical and chemical heterogeneities. Fine fragments smaller than a few

Plate 3. SEIs of three typical fragments of sample DR3A1. (a) Group "outer". A number of pores are observed in this fragment, however, such pores are not observed on the lower two surfaces. (b) Group "middle". Surrounded by clear and smooth surfaces. (c) Group "inner". Abundant phenocrysts surrounded by haloes are observed. A plagioclase phenocryst indicated by an arrow is magnified in Plate 4.

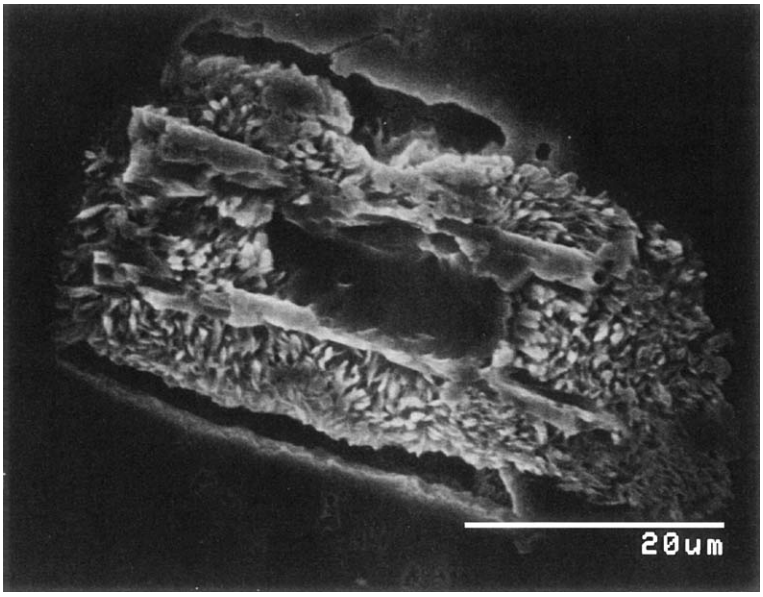

Plate 4. Magnified SEM image around a phenocryst: magnified position in this plate is indicated by an arrow in Plate 3(c).

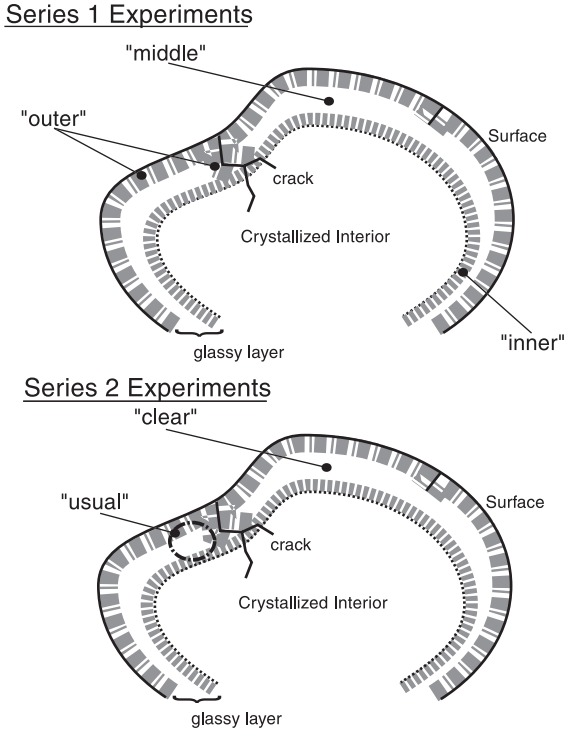

Fig. 1. Schematic drawing of positions of sub-groups within an ideal pillow fragment. (a) In Series 1 experiments. (b) In Series 2 experiments.

tenths of millimeters in size were randomly selected from residuals of the groups ‘‘usual’’ and ‘‘clear’’, remained after selection and cleaning for noble gas analyses. They were re-crushed into fragments finer than 0.1 mm: the dimension of the sample cell limits the sample size, which is 0.3 mm thick. Fragments were gently dried for a half-day at a temperature below 50 °C.

3. Experimental

3.1. Noble gas analysis

Three series of experiments were performed, as the Series 1 experiment being the main one and Series 2 and 3 as supplements. The conventional stepwise heating method was mainly applied to extract noble gases. A crushing gas extraction was also applied in the Series 3. The brief outline of the analytical procedure is summarized below and more details are described in Hanyu et al. (1999).

Gas extraction and purification lines were baked for more than 24 h at a temperature above 200 °C. Baking temperatures of sample crushers and glass sample holder were 150 °C and continued a few

Table 2a
Noble gas abundances of Indian MORBs

Sample weight (g)	T (°C)	^{4}He (10^{-6} cm^3/g)	^{20}Ne (10^{-10} cm^3/g)	^{36}Ar (10^{-11} cm^3/g)	^{40}Ar (10^{-7} cm^3/g)	^{84}Kr (10^{-12} cm^3/g)	^{132}Xe (10^{-13} cm^3/g)	$^{40}Ar^*$ (10^{-7} cm^3/g)	$^{4}He/^{40}Ar^*$
Series 1									
DR3A1 middle	400	2.99	0.22	1.47	0.041	0.32	0.28	n.d.	–
0.8792	1000	6.71	1.11	15.6	12.7	5.75	6.35	12.2	5.5
	1500	0.001	0.11	4.70	3.38	1.92	3.18	3.24	0.003
	Total	9.70	1.44	21.8	16.1	7.99	9.81	15.5	6.3
DR3A1 outer	400	1.95	0.82	10.8	0.322	2.16	1.14	0.003	6500
0.6660	1000	4.98	1.24	17.1	11.9	5.43	5.46	11.4	4.4
	1500	0.001	0.07	3.89	3.57	1.46	2.40	3.45	0.003
	Total	6.93	2.12	31.8	15.8	9.05	9.00	14.9	4.7
DR3A1 inner	400	0.829	1.67	2.90	0.089	0.66	0.24	0.003	2800
0.5429	1000	5.68	5.01	6.67	5.88	3.08	3.40	5.68	10.0
	1500	0.001	0.17	4.30	2.87	1.74	2.19	2.74	0.004
	Total	6.51	6.85	13.9	8.84	5.47	5.83	8.43	7.7
Series 2									
DR1A1 usual	500	0.116	10.3	6.34	0.192	1.27	0.10	0.003	390
0.2071	1000	6.48	25.3	49.1	3.05	7.25	4.98	1.60	41
	1500	n.d.	0.20	48.8	2.35	54.7	220	0.907	0
	Total	6.60	35.8	104	5.59	63.2	225	2.51	26.3
DR1A1 clear	400	3.11	0.39	n.d.	0.004	0.04	0.11	–	–
0.8239	1000	11.6	1.72	5.11	3.09	1.60	2.09	2.94	39
	1500	0.001	n.d.	1.54	0.599	0.72	1.74	0.553	0.018
	Total	14.7	2.12	6.65	3.69	2.36	3.95	3.49	42
DR6A1 usual	350	0.128	0.46	1.28	0.042	0.45	0.80	0.004	320
0.2413	900	17.3	8.11	51.7	9.88	9.49	8.54	8.35	21
	1500	0.016	0.30	(2.6)	1.76	3.68	6.25	1.68	0.095
	Total	17.4	8.87	55.6	11.7	13.6	15.6	10.0	17.4
DR6A1 clear	400	0.951	0.19	2.18	0.205	0.96	1.22	0.140	68
1.2527	1000	7.54	1.69	14.5	7.76	6.21	6.61	7.33	10.3
	1500	0.010	2.02	43.4	2.70	14.6	16.4	1.42	0.070
	Total	8.50	3.90	60.1	10.7	21.7	24.2	8.89	9.6
Series 3									
DR6A1c	Crush	1.12	1.43	43.5	4.39	11.8	6.04	3.10	3.6
0.4331									
DR25A1b#2	Crush	0.539	2.49	78.4	4.43	19.5	7.13	2.12	2.5
0.2325									
DR25A1b#1	Crush	2.03	3.61	105	10.5	23.1	8.74	7.34	2.8
0.2638									
DR25A1c#1	400	1.98	n.d.	0.12	0.004	0.10	0.29	–	–
0.9343	1000	9.05	1.04	10.3	16.1	4.00	3.82	15.8	5.7
	1500	0.002	0.46	15.1	5.24	5.82	8.39	4.79	0.004
	Total	11.6	1.50	25.5	21.4	9.91	12.5	20.6	5.4
DR25A1c#2	400	2.05	0.04	n.d.	n.d.	n.d.	n.d.	–	–
0.8729	1000	9.43	1.00	9.92	16.0	3.87	4.71	15.7	6.0
	1500	0.002	n.d.	3.16	4.55	1.88	3.97	4.45	0.004
	Total	11.5	1.04	13.1	20.5	5.76	8.68	20.1	5.7
DR25A1c#2-2	400	0.115	0.01	n.d.	n.d.	n.d.	0.17	n.d.	–
0.3890	1000	4.22	1.45	4.51	6.37	2.49	4.82	6.24	6.8
	1500	0.001	0.17	3.12	3.44	2.25	5.71	3.35	0.003
	Total	4.34	1.63	7.64	9.81	4.74	10.7	9.59	4.5

Table 2a (*continued*)

Typical blank	T (°C)	^{4}He (10^{-6} cm^3)	^{20}Ne (10^{-10} cm^3)	^{36}Ar (10^{-11} cm^3)	^{40}Ar (10^{-7} cm^3)	^{84}Kr (10^{-12} cm^3)	^{132}Xe (10^{-13} cm^3)
	~ 500	0.004	0.20	0.12	0.003	0.03	0.09
	1000	0.004	0.12	0.16	0.004	0.04	0.15
	1500	0.003	0.14	0.25	0.01	0.06	0.11
	Crush	0.0001	0.03	0.29	0.01	0.13	0.44

^{40}Ar* means radiogenic ^{40}Ar. "n.d.": significantly lower than blank level; "–": not analyzed. Experimental uncertainties in amounts are generally about 5% for Ar and 10% for the others (2σ), respectively, estimated from the air calibration reproducibility. Typical variations in blank levels are less than 20%, 25% and 30% for up to 500, 1000 and 1500 °C fractions, respectively.

hours longer after the end of line baking. A stepwise heating method was applied to gas extraction in three stages at ~ 500, 1000 and 1500 °C for 45, 45 and 30 min, respectively. Crushers were heated at 120 °C during gas extraction. Crushed samples were sieved out by using an 80-mesh sieve (ca. 0.2 mm) in order to estimate the efficiencies of crushing. Purifications were performed by two- (for crushing) or three-stage (for heating) titanium–zirconium getters heated at 700–800 °C. Five noble gases (He, Ne, Ar, Kr and Xe) were separated from each other using cold traps with activated charcoal and a cryogenic pump.

Measurements were performed on a sector-type mass spectrometer (VG-5400; installed at Earthquake Research Institute, The University of Tokyo). The absolute sensitivity of Ar was determined by measuring two standard samples of MMhb-1 hornblende (Samson and Alexander, 1987) and EB-1 biotite (Iwata, 1997), with a reproducibility of less than 2%. By measuring the calibrated standard air and assuming atmospheric abundances, the relative sensitivities of He/Ar, Ne/Ar, Kr/Ar and Xe/Ar were determined. Experimental uncertainties in the amounts were estimated to be about 5% for Ar and 10% for He, Ne, Kr and Xe, respectively, based on the reproducibility for the standard gas measurements. He isotope ratios were calibrated by repeated measurements of the standard gas (^{3}He/^{4}He = 5.81 ± 0.28R_A) from Kaminoyama well, Yamagata, Japan during a series of experiments. For the other noble gases, measured isotopic ratios were calibrated by repeated measurements of standard gases of diluted air and corrected for blanks. Typical blanks are listed in Tables 2a–2c. Measured isotope ratios were applied for the blank correction of Ne isotopic ratios by taking 20%, 25% and 33% variations of the blank level into account for up to 500, 1000 and 1500 °C fractions, respectively. For the correction of Xe isotope ratios, 25% variation of blank level has been applied.

3.2. Refractive index measurements

Refractive index measurements of glasses were performed by the RIMS-86 system after the modified thermal immersion method (Danhara et al., 1992) installed at the Department of Earth Science, College of Humanities and Sciences, Nihon University. This method utilizes the dependence of the refractive index on temperature, which is caused by the thermal expansion of an immersion liquid. Sample grains were loaded into a glass cell with the immersion liquid whose index parameter is adjusted to be larger than those of the samples at a low temperature (at 20 °C) and smaller at a high temperature (at 60 °C). The temperature of the cell is automatically controlled and changed cyclically. When the index of the immersion liquid becomes identical with that of the sample, the sample image is faded into the liquid optically and the index of the sample is calculated from the temperature by a microcomputer with a signal sent by an observer. The calibration of the immersion liquid has been performed by using artificial homogeneous glasses. The reproducibility is checked by repeated analyses of the calibrated standard sample of homogeneous tephra glass (the Aira AT which has a variation refractive index less than 0.05% as 1σ; Yokoyama et al., 1986). For statistical treatment and estimation of reproducibility, more than 10 grains were randomly selected and more than two points were measured in each grain.

Table 2b
Isotope ratios of He, Ne and Ar for Indian MORBs

Sample weight (g)	T (°C)	$^{3}He/^{4}He$ (R_A)	±	$^{20}Ne/^{22}Ne$	±	$^{21}Ne/^{22}Ne$	±	$^{38}Ar/^{36}Ar$	±	$^{40}Ar/^{36}Ar$	±
Series 1											
DR3A1 middle	400	8.78	0.68	14.5	3.4	0.0304	0.0096	0.1869	0.0131	279	20
0.8792	1000	8.32	0.62	12.47	1.44	0.0529	0.0074	0.1886	0.0015	8130	190
	1500	–		–		–		0.1900	0.0069	7190	250
	Total	8.46	0.48	12.77	1.33	0.0496	0.0065	0.1887	0.0021	7390	160
DR3A1 outer	400	8.82	0.69	9.81	0.72	0.0303	0.0041	0.1858	0.0023	298.1	5.5
0.6660	1000	8.01	0.60	11.99	0.81	0.0473	0.0064	0.1893	0.0022	6960	160
	1500	–		–		–		0.1899	0.0116	9190	500
	Total	8.24	0.47	11.01	0.56	0.0397	0.0041	0.1880	0.0019	4970	230
DR3A1 inner	400	8.20	0.90	11.61	1.30	0.0349	0.0053	0.1852	0.0056	306	11
0.5429	1000	8.06	0.44	10.96	0.49	0.0365	0.0023	0.1875	0.0030	8810	250
	1500	–		–		–		0.1864	0.0100	6670	300
	Total	8.09	0.40	11.11	0.48	0.0361	0.0022	0.1867	0.0036	6370	230
Series 2											
DR1A1 usual	500	–		–		–		–		300	68
0.2071	1000	–		–		–		–		621	25
	1500	–		–		–		–		481	53
	Total									536	28
DR1A1 clear	400	8.51	0.48	9.61	1.41	0.0277	0.0049	0.1884	0.1028	–	
0.8239	1000	8.30	0.51	11.62	0.30	0.0474	0.0035	0.1862	0.0016	6050	254
	1500	4.08	0.84	–		–		0.1874	0.0056	3889	179
	Total	8.43	0.36	11.19	0.39	0.0431	0.0030	0.1866	0.0030	5550	210
DR6A1 usual	350	8.26	1.21	–		–		–		330	150
0.2413	900	8.86	0.52	–		–		–		1910	77
	1500	3.43	0.54	–		–		–		(6840)	
	Total	8.85	0.52							2100	370
DR6A1 clear	400	9.51	0.58	9.63	0.29	0.0290	0.0051	0.1869	0.0013	939	38
1.2527	1000	8.65	0.50	11.38	0.16	0.0468	0.0019	0.1866	0.0011	5370	220
	1500	4.60	1.17	10.02	0.19	0.0285	0.0013	0.1889	0.0017	622	26
	Total	8.74	0.45	10.54	0.13	0.0358	0.0011	0.1883	0.0012	1780	130
Series 3											
DR6A1c 0.4331	Crush	8.55	0.70	10.16	0.42	0.0301	0.0034	0.1879	0.0016	1008	13
DR25A1b#2 0.2325	Crush	8.58	0.77	10.26	0.43	0.0310	0.0031	0.1868	0.0016	565.4	6.1
DR25A1b#1 0.2638	Crush	8.47	0.68	9.72	0.34	0.0293	0.0021	0.1878	0.0019	993	17
DR25A1c#1	400	8.51	0.51	–		–		–		–	
0.9343	1000	8.20	0.45	12.63	0.84	0.0582	0.0063	0.1879	0.0068	15,690	560
	1500	–		9.78	1.19	0.0294	0.0057	0.1893	0.0027	3473	97
	Total	8.25	0.38	11.59	0.70	0.0477	0.0046	0.1887	0.0032	8380	230
DR25A1c#2	400	8.55	0.50	–		–		–		–	
0.8729	1000	8.08	0.42	12.35	1.27	0.0553	0.0074	0.1884	0.0038	16,090	620
	1500	–		–		–		0.1888	0.0076	14,410	540
	Total	8.17	0.36	12.35	1.27	0.0553	0.0074	0.1885	0.0034	15,680	480
DR25A1c#2-2	400	8.72	0.34	–		–		–		–	
0.3890	1000	8.33	0.17	11.81	0.38	0.0562	0.0029	0.1882	0.0079	14,120	540
	1500	–		10.4	2.2	0.080	0.018	0.190	0.030	11,000	1300
	Total	8.34	0.17	11.63	0.43	0.0591	0.0035	0.189	0.013	12,850	610
Air		1		9.80		0.029		0.188		295.5	

4. Results

4.1. Noble gas signatures related with sample textures: Series 1 experiments

In order to estimate the relationship with textures, the noble gas signatures of the three groups were examined in detail. Elemental abundance patterns for the three groups are shown in Fig. 2. Here, total amounts of three temperature fractions of stepwise heating are plotted and used for calculation of elemental ratio since it might be possible that gases dissolved in glass matrices cause fractional releases by diffusion: the diffusivity of He is the highest but that of Xe is the lowest among noble gases (e.g. Ozima and Podosek, 2002). All three groups show typical MORB patterns: He enrichment and gradual depletion toward heavy noble gases (Fig. 2a). These patterns are almost parallel to those of the popping rock, 2ΠD43 (Staudacher et al., 1989; Moreira et al., 1998). This is significant since many workers regarded the popping rock as a representative of an unfractionated noble gas composition of MORB parental magma, at least under a low degree of melting condition (e.g. Staudacher et al., 1989). Its noble gas abundance varies by more than one order of magnitude as reported so far (e.g. Staudacher et al., 1989; Moreira et al., 1998). Fig. 2b shows relative abundances to the ^{36}Ar in samples normalized to that of the popping rock reported in Moreira et al. (1998): the values of experiment 1 are adopted due to much pristine signature as represented by the higher ^{40}Ar/^{36}Ar. The ^{36}Ar abundance of DR3A1 is lower than that of the popping rock by almost two orders of magnitude, whereas He and Xe abundance is much close to those of the popping rock. Thus, all three groups show U-shaped patterns due to the enrichment of He and Xe. Such U-shaped patterns could be interpreted as a result of fractional crystallization under a low vesicularity condition (Spasennykh and Tolstikhin, 1993).

In their detailed characters, there are significant differences among the three groups (Fig. 2a). The ‘‘outer’’ group shows a slight enrichment in Ne and Ar compared to the ‘‘middle’’ group. Since ^{20}Ne and ^{36}Ar show an enrichment with similar degrees in the ‘‘outer’’ group, the normalized Ne/Ar ratio becomes similar to that of the ‘‘middle’’ group. This ^{36}Ar enrichment causes a significantly lower He/Ar, Kr/Ar and Xe/Ar ratios for the ‘‘outer’’ group than those for the ‘‘middle’’ group. Besides clear overabundance of Ne, the ‘‘inner’’ group has the least amount of released noble gases with similar abundance pattern to ‘‘middle’’ group.

The release patterns of noble gases reflect the state of trapped gases and the origin of different component. All three groups show similar release patterns of ^{40}Ar/^{36}Ar: a quite low ratio (almost atmospheric, ca. 300) in the first fraction (400 °C) and much higher ratios of around 8000 in both the second (1000 °C) and the third (1500 °C, fusion) fractions. Fig. 3 shows the ^{40}Ar/^{36}Ar ratio released in each temperature fraction against the cumulative amount of released ^{36}Ar.

The ‘‘outer’’ group shows the largest amount of ^{36}Ar among the three groups, releasing one third of the total ^{36}Ar in the first step with almost the atmospheric isotope composition. This atmospheric Ar released at a low temperature might reflect the addition of an atmospheric component related with a low temperature phenomenon such as alteration and/or weathering in seawater. However, simple seawater addition cannot explain the elemental abundance pattern as shown in Fig. 2b, because the addition of seawater changes the Ne/Ar ratio.

In the ‘‘middle’’ group, only little gases were released at 400 °C, whereas almost three quarters of the total amount were degassed in the 1000 °C fraction. Besides gases released at 400 °C, both ‘‘middle’’ and ‘‘outer’’ group contain similar amounts of ^{36}Ar. The broken line in Fig. 3a has a slope parallel with the slope of the ‘‘outer’’ group, starting from the low temperature fraction of the ‘‘middle’’ group. This line also suggests that Ar components in both the ‘‘middle’’ and the ‘‘outer’’ group have almost the same isotope ratios indicating the common origin. This means that the ‘‘middle’’ group contains a single, probably magmatic noble gas component. The closed

Note to Table 2b:
Variations (50%) of blank levels have been applied to blank correction except for Ne. For Ne, actual variation of blank levels has been applied since deviations for Ne are smaller compared to those for He or Ar. The isotope compositions of air are referred from Ozima and Podosek (2002).

Table 2c
Xe isotopes for Indian MORBs

Sample	T (°C)	$^{124}Xe/^{130}Xe$		$^{126}Xe/^{130}Xe$		$^{128}Xe/^{130}Xe$		$^{129}Xe/^{130}Xe$		$^{131}Xe/^{130}Xe$		$^{132}Xe/^{130}Xe$		$^{134}Xe/^{130}Xe$		$^{136}Xe/^{130}Xe$	
			±		±		±		±		±		±		±		±
Series 1																	
DR3A1 middle	1000	0.029		0.0194		0.466		6.66		5.22		6.63		2.67		2.29	
		0.012		0.0052		0.038		0.35		0.31		0.40		0.15		0.13	
	1500	0.035		0.027		0.485		6.53		5.15		6.60		2.59		2.204	
		0.015		0.012		0.040		0.30		0.27		0.30		0.13		0.094	
DR3A1 outer	1000	0.0257		0.0253		0.474		6.65		5.14		6.58		2.657		2.276	
		0.0076		0.0073		0.040		0.23		0.25		0.26		0.097		0.099	
	1500	0.040		0.020		0.449		6.37		5.15		6.47		2.50		2.22	
		0.016		0.015		0.039		0.50		0.46		0.47		0.17		0.14	
DR3A1 inner	1000	0.026		0.027		0.496		6.79		5.22		6.78		2.73		2.36	
		0.014		0.017		0.092		0.57		0.41		0.51		0.22		0.23	
	1500	0.033		0.018		0.491		6.72		5.14		6.62		2.72		2.33	
		0.023		0.018		0.054		0.51		0.53		0.63		0.28		0.23	
Series 2																	
DR1A1 clear	1000	0.038		0.020		0.464		6.67		5.26		6.41		2.58		2.23	
		0.016		0.018		0.079		0.65		0.55		0.70		0.31		0.35	
	1500	0.024		0.019		0.490		6.70		5.43		6.99		2.68		2.35	
		0.026		0.020		0.059		0.56		0.28		0.42		0.22		0.21	
DR6A1 clear	1000	0.0245		0.0228		0.482		6.59		5.18		6.60		2.61		2.230	
		0.0088		0.0087		0.035		0.20		0.23		0.23		0.11		0.092	
	1500	0.0250		0.0185		0.461		6.35		5.14		6.49		2.56		2.183	
		0.0060		0.0069		0.025		0.24		0.20		0.24		0.10		0.084	
Series 3																	
DR6A1c	Crush	0.035		0.021		0.487		6.41		5.12		6.50		2.53		2.15	
		0.016		0.013		0.066		0.54		0.44		0.54		0.25		0.23	
DR25A1b#2	Crush	0.027		0.024		0.474		6.53		5.25		6.64		2.66		2.28	
		0.019		0.015		0.087		0.84		0.66		0.84		0.36		0.36	
DR25A1b#1	Crush	0.037		0.022		0.484		6.35		5.19		6.44		2.58		2.18	
		0.017		0.014		0.056		0.62		0.53		0.64		0.28		0.25	
DR25A1c#1	1000	0.017		0.021		0.481		6.64		5.12		6.58		2.64		2.23	
		0.011		0.014		0.066		0.31		0.20		0.23		0.13		0.11	
	1500	0.0184		0.0261		0.477		6.64		5.05		6.57		2.65		2.249	
		0.0063		0.0094		0.026		0.29		0.17		0.27		0.12		0.097	
DR25A1c#2	1000	0.0185		0.025		0.473		6.82		5.12		6.64		2.71		2.28	
		0.0092		0.016		0.028		0.29		0.39		0.33		0.22		0.16	
	1500	0.019		0.0204		0.487		6.91		5.13		6.69		2.75		2.30	
		0.010		0.0044		0.050		0.31		0.30		0.33		0.15		0.11	
DR25A1c#2-2	1000	0.071		0.023		0.476		6.84		5.36		6.68		2.67		2.28	
		0.042		0.012		0.052		0.16		0.15		0.32		0.14		0.14	
	1500	0.063		0.0187		0.447		6.90		5.38		6.63		2.74		2.28	
		0.026		0.0076		0.039		0.35		0.33		0.39		0.16		0.17	
Air		0.0235		0.0221		0.470		6.48		5.19		6.59		2.56		2.17	

Analytical uncertainties are shown as 1σ including blank correction. In blank correction, 25% variations of blank levels are applied, which is estimated from actual variation of blanks. Xe isotopes of all fractions of "usual" samples in the Series 2 and of the lowermost temperature fractions of all other samples were not analysed. The isotope compositions of Air are taken from Staudacher and Allègre (1982).

star in Fig. 3a indicates the estimated magmatic component which contains the same amount of ^{36}Ar as "middle" group with the highest $^{40}Ar/^{36}Ar$ of "middle" group. Such magmatic component should be derived from a mixing between the atmospheric component and the source material of the MORB endmember: $^{40}Ar/^{36}Ar$ ranges from 25,000 to 44,000 (Moreira et al., 1998). It is a subject of further studies whether significantly contaminated source material (down to 9000 of $^{40}Ar/^{36}Ar$) really exists beneath the sampled area (e.g. Sarda et al., 1999).

The "inner" group shows lower amounts of released gases than the other groups, especially in the 1000 °C fraction. After subtracting ^{36}Ar in the 400 °C fraction as the atmospheric component from total ^{36}Ar, it becomes almost half as much as that of the "middle" group. This might be due to the loss of magmatic components since all these three parts were solidified from an identical extrusion of magma.

Fig. 4a–c shows release patterns of noble gases against degassing temperatures. All noble gases generally show similar release patterns, released mostly in the 1000 °C fraction. Since He and Ne show greater mobility compared to Ar due to their small masses and atomic radii, they are usually more released at low temperatures, up to 1000 °C. Contrarily, Kr and Xe are less mobile and they are still released to some extent at 1500 °C. The simple pattern of "middle" group could be interpreted as a result of diffusion process since amounts of released gases are proportional to the square root of a diffusion constant. Compared to the "middle" group, the "outer" group releases larger proportions of gases up to 400 °C. Especially, Ne with the atmospheric composition accounts for almost 40% of the total released Ne. Since larger proportions of Ne and Ar were released at

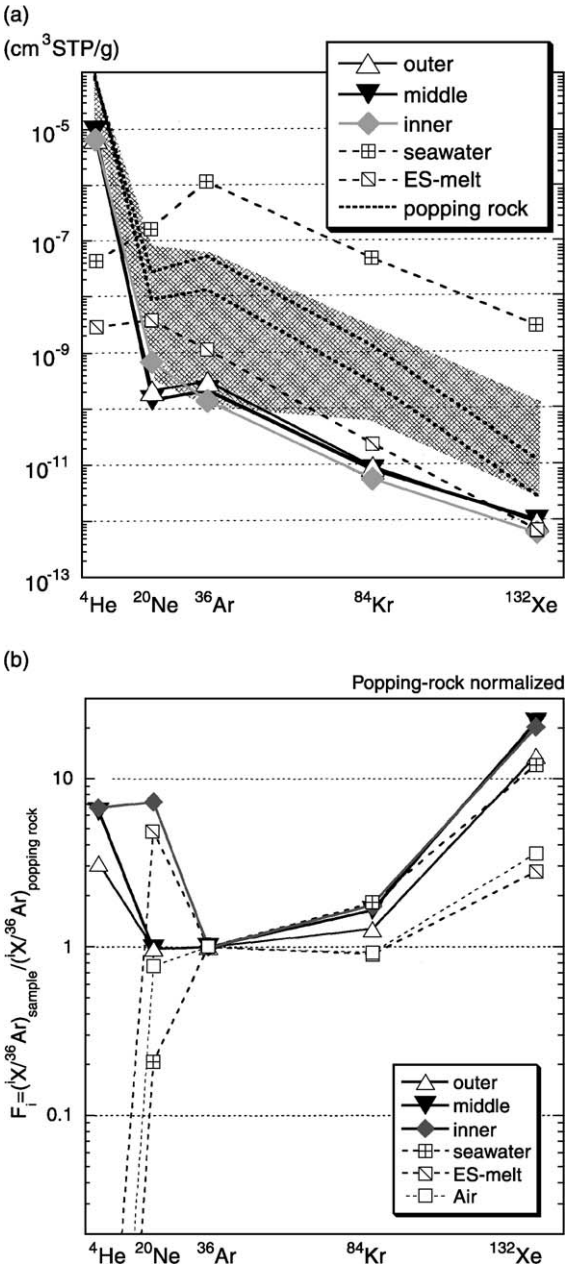

Fig. 2. (a) Noble gas abundance patterns for groups "outer", "middle" and "inner" of the sample DR3A1, respectively. Total amount is plotted for each group. The abundance pattern of deep seawater (seawater) and tholeiitic MORB melt equilibrated with the deep seawater (ES-melt) are also plotted as broken lines. Solubility data used for calculation are taken from Table 4.6 of Ozima and Podosek (2002) for deep seawater and from Fig. 13 of Carroll and Webster (1994) for MORB melt. The range of the popping-rock (2ΠD43) is also shown by hatches (Staudacher et al., 1989; Moreira et al., 1998). As an example, the patterns reported in Moreira et al. (1998) are plotted as dotted lines. (b) Normalized noble gas abundance patterns of three groups. Normalized values of $(^4He/^{36}Ar)_{popping\ rock}$, $(^{20}Ne/^{36}Ar)_{popping\ rock}$, $(^{84}Kr/^{36}Ar)_{popping\ rock}$ and $(^{132}Xe/^{36}Ar)_{popping\ rock}$ are 7000, 0.680, 0.0223 and 0.000208, respectively (calculated from Experiment 1 reported in Moreira et al., 1998). The patterns of deep seawater, ES-melt and air are also plotted. $(^4He/^{36}Ar)_{contaminant}/(^4He/^{36}Ar)_{popping\ rock}$ of deep seawater, ES-melt and air are 5.34×10^{-6}, 3.58×10^{-4} and 2.37×10^{-5}, respectively.

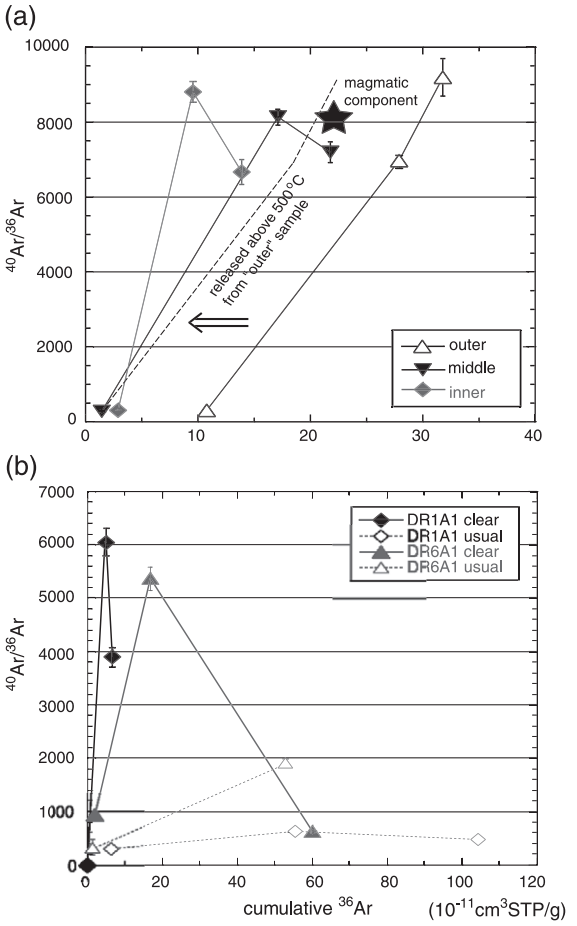

Fig. 3. Release patterns of Ar plotted on the diagram of cumulative ^{36}Ar vs. $^{40}Ar/^{36}Ar$ ratio for (a) Series 1 and (b) Series 2 experiments, respectively. Unless indicated, analytical uncertainties are comparable to the size of the symbols. In (a), the broken line has a slope parallel with the slope of the "outer" group, starting from the low temperature fraction of the "middle" group. The filled star indicates an inferred magma-derived component that was observed in the "middle" and the "outer" group as similar end point of both connected lines. In (b), because of small release of Ar and high blank, the $^{40}Ar/^{36}Ar$ was neither well determined nor plotted in the 1500 °C fraction of DR6A1 "usual". Since the amount of released ^{36}Ar is indistinguishable from the blank level, the data of the 400 °C fraction of DR1A1 "clear" is plotted at the origin.

400 °C compared to He, this pattern could not be interpreted as simple diffusion pattern under uniform distribution. One possible explanation is heterogeneous distribution of Ne and Ar: abundant Ne and Ar with the atmospheric compositions are distributed near the surface of grains. The "inner" group released significantly larger proportions of Kr and Xe in the highest temperature fraction.

Within analytical uncertainties, He isotope compositions are indistinguishable among the three groups as total values. Ne isotopes for both the "outer" and "inner" groups are lower than those for the "middle" group as total values. Since abundant Ne with the almost atmospheric composition was released in the 400 °C fraction of the "outer" group, total $^{20}Ne/^{22}Ne$ decreases to 11. In the "middle" group, Ne was released little at 400 °C. Hence, the isotope ratio is

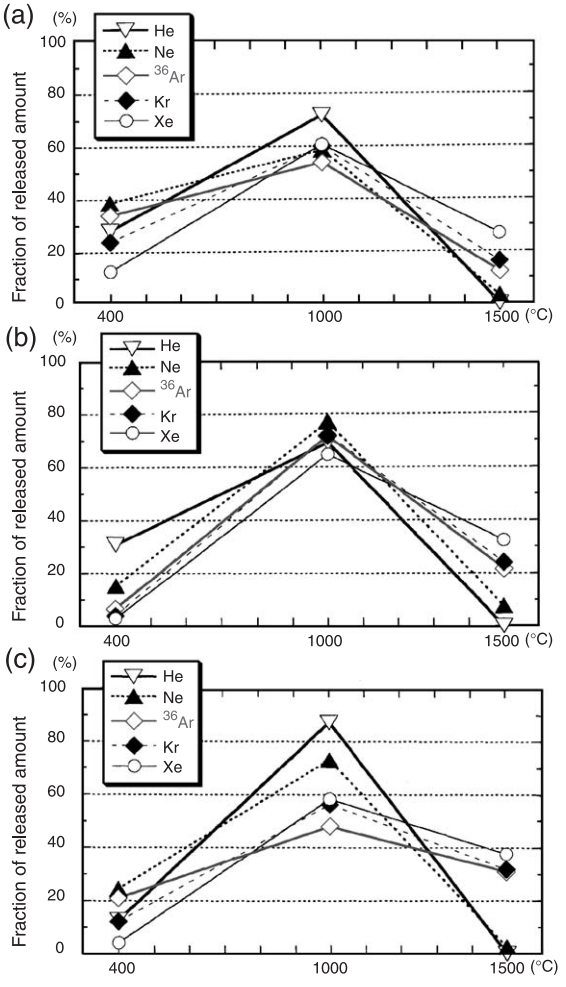

Fig. 4. Release patterns of all noble gases for the (a) outer, (b) middle and (c) inner groups in Series 1 experiment. The patterns are shown as relative proportion of released amount in each temperature fraction to the total amount for each noble gas.

not plotted in the figure due to its large uncertainty. Strongly enriched Ne in the "inner" group shows a $^{20}Ne/^{22}Ne$ of ~ 11 even in the 1000 °C fraction (Fig. 5). This implies that the atmospheric component is well mixed with the magmatic component in the "inner" group.

Although analytical uncertainties are large, Xe isotopes seem to show typically 3% excesses exceeding 1σ uncertainties in the 1000 °C fraction at mass numbers of 129, 134 and 136 relative to the atmospheric compositions (Table 2c). Kr isotopes of the three groups have atmospheric compositions within analytical uncertainties.

$^{40}Ar^*$ (radiogenic ^{40}Ar) and $^{4}He/^{40}Ar^*$ ratio are useful tracers to evaluate the contribution of the magmatic component. Here, $^{40}Ar^*$ is calculated by subtracting the atmospheric ^{40}Ar from the total amount. In the 400 °C fraction, although up to 30% of He are released, the amounts of released $^{40}Ar^*$ are negligible. Thus, $^{4}He/^{40}Ar^*$ ratios are quite high in the lower temperature fractions and decrease to almost zero in the higher temperature fractions (Table 2a). As total values, both the "outer" and the "middle" groups show typical MORB values. However, the "inner" group has almost a half amount of $^{40}Ar^*$ and a higher $^{4}He/^{40}Ar^*$ ratio than the other groups. This implies that "inner" position lost magmatic component via vesicle-loss.

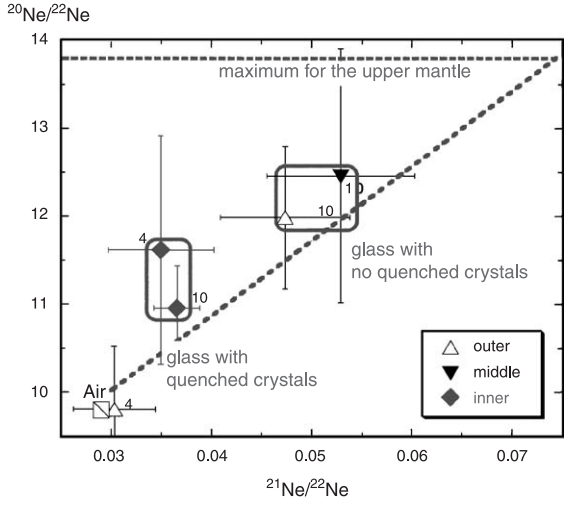

Fig. 5. Ne three-isotope plot for three sub-groups of the sample DR3A1 in Series 1 experiments. Broken lines show the correlation line of the Atlantic MORB (Sarda et al., 1988) and the upper limit of mantle $^{20}Ne/^{22}Ne$ estimated from that of solar Ne. The numerical figure at each symbol indicates a degassing temperature in the unit of 100 °C.

4.2. Comparison between new sample selection and usual one: Series 2

Two sets of "usual" and "clear" samples for the Series 2 were compared with the results for the Series 1. We have focused at first on Ar release patterns due to its sensitivities for atmospheric contamination. Fig. 3b shows the $^{40}Ar/^{36}Ar$ ratio in each temperature fraction against the cumulative amount of released ^{36}Ar. Because of small release of Ar and high blank, the $^{40}Ar/^{36}Ar$ was neither well determined nor plotted in the 1500 °C fraction of DR6A1 "usual". Since the amount of released ^{36}Ar is indistinguishable from the blank level, the data of the 400 °C fraction of DR1A1 "clear" is plotted at the origin. For all samples, the middle temperature fractions show the highest $^{40}Ar/^{36}Ar$ ratios, as is the case for the "middle" group of the Series 1. The samples of group "usual" show much lower $^{40}Ar/^{36}Ar$ ratios compared to those of the group "clear". Especially, DR6A1 "usual" does in all the three temperature fractions.

Although high $^{4}He/^{40}Ar^*$ implies extensive vesicle-loss, the "clear" groups have almost identical values of $^{4}He/^{40}Ar^*$ ratios both in the 1000 °C fraction and as total (Sarda and Moreira, 2002), which suggests that "clear" samples contain a dominant noble gas component. Although their release patterns are not completely interpreted as diffusion-controlled pattern (see Section 5.2), the "clear" groups resemble the "middle" group of the Series 1. Furthermore, the stepwise heating method is proved to be little effective in removing the atmospheric component unless careful precautions are taken during sample selection. The sample DR6A1 "clear" shows a relatively large amount of ^{36}Ar released with a quite low $^{40}Ar/^{36}Ar$ ratio in the highest temperature fraction. This point shall be discussed later.

4.3. Crushing and supplements: Series 3

The $^{40}Ar/^{36}Ar$ of heated c#2 and #1 in the 1000 °C fraction are indistinguishable from each other, of which values are $16{,}100 \pm 600$ and $15{,}700 \pm 600$,

respectively. In our previous study (Kumagai and Kaneoka, 1998), the outermost b#1 showed a significantly low $^{40}Ar/^{36}Ar$ ratio in the 1000 °C fraction. This difference might be resulted from the usage of a gentle ultrasonic bath with diluted HNO_3. The $^{40}Ar/^{36}Ar$ of c#2-2 is 14,120 ± 540 in the 1000 °C fraction, which still overlaps with c#2 within 2σ uncertainties. These values are also indistinguishable from that of b#2, 17,500 ± 5600 (Kumagai and Kaneoka, 1998), which suggests that there might be a certain magmatic component in the pillow fragment of DR25A1 as in DR3A1. The simple release pattern of c#2 reflecting diffusion also supports this interpretation.

Crushed samples released significant amounts of gases, especially, ^{36}Ar released up to twice as much as the total amount of heating extraction. In the case of Kr, almost equal amounts with those by heating experiment were released. Such large amount of Ar and Kr might be related with the atmospheric contaminant as indicated with a significantly low $^{40}Ar/^{36}Ar$. This strange result might be resulted from differences of sample sizes used in crushing experiments. As described in Section 2.1 and summarized in Table 1, significantly large aliquots as available were used for crushing experiment in order to obtain higher efficiencies of crushing. As an alternative possibility, this over-abundance of ^{36}Ar might be resulted from a heterogeneous distribution of atmospheric contamination. On the other hand, the efficiencies of crushing are estimated to be approximately 50% from measuring their grain sizes after extractions: grains finer than 0.2 mm sieving are defined as crushed. This result indicates that 50% of the large vesicle gas was liberated at most. Actually, He, $^{40}Ar^*$, Xe and most of Ne released were less than half of the amount released by heating, which is easily explained by the efficiency of crushing.

Fig. 6 shows the normalized abundance patterns of crushing experiments as in Fig. 2b. The abundance pattern obtained by crushing extraction is much closer to those of the Air, the ES-melt and seawater. Here, the ES-melt is calculated as tholeiitic MORB melt equilibrated with the deep seawater: solubility data used for calculations are taken from Table 4.6 of Ozima and Podosek (2002) for seawater and from Fig. 13 of Carroll and Webster (1994) for MORB melt. Contrarily, the values by heating extraction

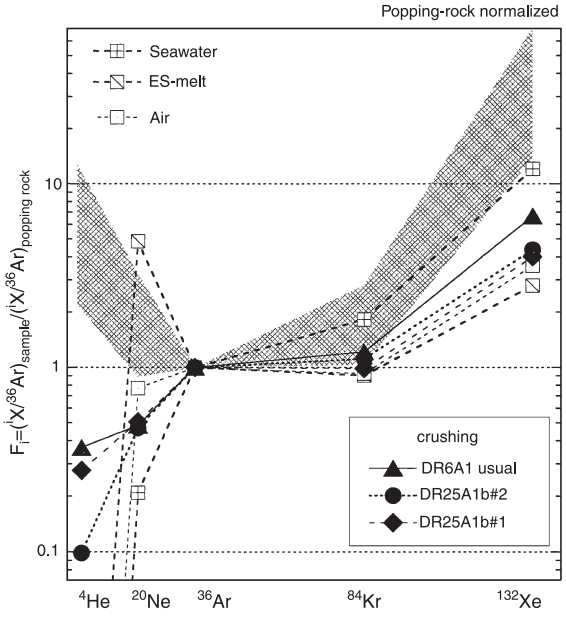

Fig. 6. Normalized noble gas abundance patterns of crushing extractions of Series 3 experiments. Range of heating results is shown by hatches. The patterns of deep seawater, ES-melt and air are also plotted.

show similar patterns to the "middle" group of Series 1 as indicated by hatches. Especially, the normalized $^{20}Ne/^{36}Ar$ of c#1 and c#2 are quite close to the $^{20}Ne/^{36}Ar$ for the "middle" group.

Additionally, the $^4He/^{40}Ar^*$ ratios resulting from crushing experiments neither agree with those of each temperature fraction nor total values by step heating. The $^4He/^{40}Ar^*$ by crushing experiments vary from 2.5 to 3.6. These are close to less fractionated vesicle component (Sarda and Moreira, 2002) and significantly lower than those of step heating ranging from 5.7 to 21 as the total one or in the main release fraction at 1000 °C.

In heating experiments of DR25A1, the $^4He/^{40}Ar^*$ ratios are rather similar ranging from 4.5 to 5.7 as total and from 5.7 to 6.7 for the main fraction released at 1000 °C, respectively. All the $^4He/^{40}Ar^*$ of these experiments overlap almost completely with those of DR25A1b ranging from 5.7 to 8.6. This suggests that magma-derived components distribute rather homogeneously at least in a significant part of the thick glass layer. Although the total value of $^4He/^{40}Ar^*$ for the sample c#2-2 is much lower than the range of

DR25A1b, the value of the 1000 °C fraction is within its range. This implies that significant amount of He, which should be released at low temperatures, has been escaped. Additionally, the gas amount of c#2-2 is almost half of that of #2. Furthermore, rapid decrease in the $^4He/^{40}Ar^*$ is found in our previous data associated with the precipitation of quenched microcrystals resulting in loss of magmatic gases (Kumagai and Kaneoka, 1998).

Hence, the difference in chip sizes of the samples might contribute to the variation of $^4He/^{40}Ar^*$. Large vesicles up to a few tenths of a millimeter in diameter might be preserved in plate-shape or large block samples. On the other hand, during the selection of "clear" glasses, sample fragments were crushed into pieces of much smaller size. This might destroy larger vesicles, which have a lower $^4He/^{40}Ar^*$ interpreted as a mixture of magmatic gas with vapors from seawater heated up by a magma. The effect of a heterogeneous distribution cannot be excluded completely, but should be reduced by the applied preparation scheme. This interpretation does not apply to the pair of samples DR6A1 and this point shall be discussed later.

4.4. Refractive index measurements

The refractive indices for the two sub-groups of fragments separated from DR6A1 were compared (Fig. 7). Fragments of the group "usual" show a relatively high average refractive index ($n = 1.5462 \pm 0.0021$, $N = 23$) and a broad distribution: relative variation is 0.14% 1σ. The group "clear" shows a lower average ($n = 1.5401 \pm 0.0014$, $N = 23$) and a smaller variation (0.09% 1σ). These average values are statistically different, which has been confirmed by an F-test.

Assuming that the group "clear" indicates almost the intrinsic value, an increase for the group "usual" could be explained by either of the following two phenomena. Hydration from the surface of the glassy sample is one possibility. To explain this difference by hydration alone, the additional water content required is only ca. 0.2 wt.% calculated from the difference of average refractivities between the two sub-groups divided by the specific refractivity of H_2O, 0.340 (Danhara, 1991; details are described in Appendix B). Another explanation is the oxidation

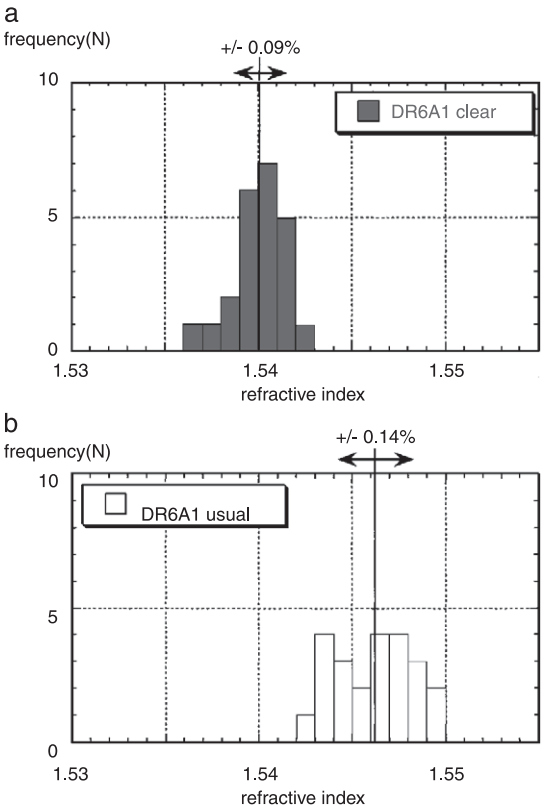

Fig. 7. Distribution of refractive indices of two groups of the sample DR6A1: (a) "clear" group; (b) "usual" group. For each group, average and standard deviation of distribution as 1σ are shown.

of Fe^{2+} to Fe^{3+}. Usually, fresh MORBs show a relatively reduced and uniform redox state with 15% Fe^{3+} of total Fe (Christie et al., 1986). The oxidization of half of Fe^{2+} into Fe^{3+} would be sufficient to explain the difference in refractivity as well as the H_2O calculation: the specific refractivity of Fe_2O_3 is 0.317. Although it is still uncertain which factor (hydration or oxidation) dominates the change in the refractive index, the analysis of refractive indices is potentially useful to check the homogeneity of a glassy sample. As a temporary working procedure for an unknown sample, further selection should be performed in case of a large dispersion for the refractive indices of e.g. 0.1% or larger. More experiments are required to utilize refractive indices as a commented for the quantitative evaluation of homogeneity.

5. Discussion

5.1. Origin and mechanism of contamination with the atmospheric component in a single pillow

To interpret the differences between measured noble gas data among the three groups of the Series 1 experiments, we assume that the erupted magma that generated DR3A1 initially had uniform noble gas signatures and that the three groups were differently affected by during- and post-eruption processes. Furthermore, we consider that the "middle" group is least affected by such processes and the best representative of a magmatic noble gas component based on the following observations as described in Sections 2.1 and 4.1: (1) optical homogeneity and isotopic uniformity (Plate 3 and Fig. 5), (2) simple release pattern controlled by diffusion (Figs. 3 and 4).

To investigate processes of contamination by atmospheric component, results for each temperature fraction for Series 1 experiments are plotted on the $^{132}Xe/^{22}Ne$–$^{36}Ar/^{22}Ne$ diagram (Fig. 8a). In this diagram, the contaminants are clearly distinguished from each other. All of the "inner" group plot very close to the ES-melt: a component derived by magma–seawater interaction. Other data make a rough linear trend from the ES-melt and the value of "middle" group is the most distant from the ES-melt among intermediate temperature fractions. Data of lower temperature fractions are scattered around a line tying the ES-melt with seawater.

The noble gas signature of the "outer" group can be explained by the addition of an atmospheric component, indicated by the increase in the amount of ^{36}Ar and Ne (Figs. 2 and 5). Although seawater is generally regarded as a source of ^{36}Ar, un-fractionated air might be also a contaminant to explain the elemental composition of the "outer" group. Although the ES-melt hardly explains the Ne/Ar ratio of the observed pattern due to its overabundance of Ne, all data of the "outer" group are scattered around a line tying between the ES-melt and seawater. Based on microscope observation, typical contaminated zone, 10 μm in thickness, is corresponding to 3 vol.% of a grain with 300 μm typically in size. This suggests that the amounts of atmospheric ^{36}Ar and ^{20}Ne derived from seawater are 4×10^{-11}, 1×10^{-11} cm^3 STP, respectively. Additionally hydration of 0.2% water for

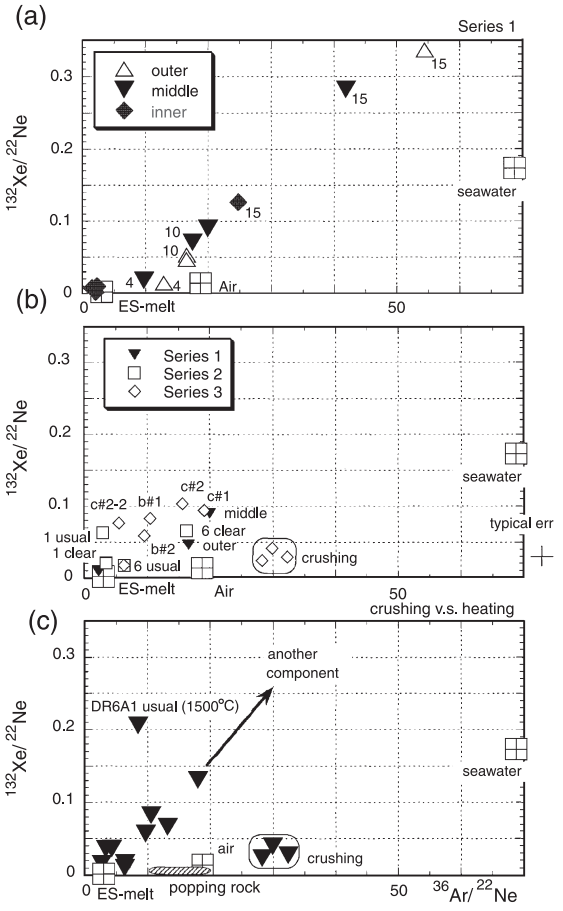

Fig. 8. Relations between the $^{36}Ar/^{22}Ne$ and the $^{132}Xe/^{22}Ne$ for (a) Series 1, (b) total values of all experiments and (c) crushing and corresponding heating extractions. Name of samples and temperature fractions for sub-plates (a) and (c) are indicated as subscription for symbols. The results of crushing experiments of Series 3 are enclosed by a frame in subfigures (b) and (c). Hatched region shows the variation of popping rock (data sources: Moreira et al., 1998; Staudacher et al., 1989; Sarda et al., 1988). Values of deep seawater, ES-melt and air are also shown.

contaminated zone of the "outer" group (Section 4.4) adds the amount of atmospheric ^{36}Ar by 1×10^{-10} cm^3 STP, which are comparable to those observed in the lower temperature fractions of the "outer" group.

The elemental abundance of the "inner" group is characterized by a strong enrichment of Ne (Fig. 2), whereas the other noble gases of the "inner" group show a decrease in their amounts. To explain this, it has been conjectured that one-third of the magmatic noble gases first escaped during the slow cooling of

magma estimated from a decrease in He of ca. 30%. Spasennykh and Tolstikhin (1993) showed that, Ne rather than Xe is strongly enriched in basaltic glass with a low vesicularity. However, if this is the case, He should show similar or even stronger enrichment than Ne. It has not been interpreted as the contamination by either the un-fractionated air or the seawater-like component because such mixing would cause a much more pronounced enrichment with ^{36}Ar than Ne resulting in a depletion of Ne. Therefore, the contamination has selectively enriched Ne, possibly related to a kinetic process. One possible contaminant is a component derived from seawater invading through cracks by diffusion because lighter noble gases, which have smaller atomic radii, show larger diffusion coefficients in a silicate than heavier ones. In this case, since relative abundance of He in seawater compared to erupted magma is 10^6 lower than that of Ne (Fig. 2a), He enrichment should be limited. Another is the ES-melt which shows a strong enrichment with Ne due to its relatively large partition coefficient between a melt and seawater. Data for ''inner'' group tightly distribute around the ES-melt, which strongly indicate the concernment of the ES-melt for contamination process. Although this would cause a weak enrichment with Ne than that of the ''inner'' sample, the value is quite close to that of ''inner'' sample (Fig. 2b).

Such an interaction has already been discussed with regard to the samples from Loihi seamount (Patterson et al., 1990, 1991). They interpreted the variations of elemental ratios as the result of the incorporation of seawater and degassing due to vesicle separation at a depth. This process does not explain the results of this study since the ''inner'' group shows the Ne increase as an absolute amount. Although Staudacher et al. (1991) pointed out that the noble gases released at low temperature are likely to include a component of surface-correlated atmospheric gases, this is not the case for present samples because $^{20}Ne/^{22}Ne$ in the middle temperature fraction is much lower than that of lower temperatures. Direct equilibrium between basaltic melt and seawater is unlikely, and some carrier or mechanism is needed in this case, possibly the drain back process of a magma that entrained seawater as suggested by Gregg et al. (2000). Contact of seawater with the inner walls of pillow lava might cause such an interaction: pillow lavas frequently have hollows whose inner wall might be still hot and not be completely solidified, containing melt within the crystal mush zone during their growth.

In contrast, the cooling rate of the ''middle'' part of glassy rind is sufficiently rapid to freeze volatile components and has less contact with seawater. Generally, He, which diffuses fastest among noble gases, has a diffusion coefficient that is by at least two orders of magnitude lower than that of the heat (e.g. Hanyu and Kaneoka, 1998). This suggests that solidification and cooling processes of a magma are too fast to lose He by diffusion. Assuming the thermal diffusivity to be 10^{-6} m^2/s, the temperature at the position of 1 cm inside from the lava surface decreases down to 500 °C within 5 s. Since the surface of glasses in direct contact with seawater is removed as the ''outer'' part approximately 1 mm in thickness, He in the ''middle'' part of the sample could be preserved typically for 10^5 years at 0 °C if extrapolating the diffusivity of He at 0 °C as 10^{-17} m^2/s after Watson (1994).

Hence, the ''middle'' part obtained by excluding of either weathering parts or quenched microcrystals from glassy fragment is suitable for noble gas analyses based on the following evidences. (1) It shows actual homogeneities indicated by small deviation of refractive index parameter. (2) It is the best representative of a magma-derived noble gas component with abundant magmatic gases (He and $^{40}Ar^*$) and least contaminated isotopic signature (the highest $^{40}Ar/^{36}Ar$). On the contrary, both the ''outer'' weathered part and the ''inner'' part including quenched microcrystals are contaminated by atmospheric component.

5.2. Distribution and conditions of magmatic and atmospheric components

There are at least two components within MORB glasses: one is characterized by high $^{40}Ar/^{36}Ar$ and relatively high $^4He/^{40}Ar^*$ ranging from 4 to 10, typically observed in ''clear'' samples including the ''middle'' group in Series 1. The other one is characterized by low $^{40}Ar/^{36}Ar$ and relatively low $^4He/^{40}Ar^*$ (around 3), typically observed in the crushing experiment. Although the release patterns of ''clear'' samples seem to be controlled by diffusion, total values of $^4He/^{40}Ar^*$ are close to those observed in the middle temperature fraction. Then, fractionation by diffusion is not so significant to cause such $^4He/^{40}Ar^*$ varia-

tions. Our SEM observation (see Section 2) indicates the occurrence of two kinds of vesicles with significant difference in their sizes in the present samples. One kind of vesicles is large (larger than 100 μm) and occasionally found, while the other has much smaller size (typically 10 μm or smaller) and observed ubiquitously. The former is not preserved during the preparation of the "clear" group. This suggests that larger vesicles with less He might have been affected by atmospheric contamination and smaller vesicles with much He would represent a less contaminated component. According to Moreira et al. (1998), early steps of stepwise crushing usually show a significantly contaminated signature but later ones show much more intrinsic ones. Although they did not focus an internal variation of $^{4}He/^{40}Ar^{*}$, there is a clear correlation between the $^{4}He/^{40}Ar^{*}$ and the $^{40}Ar/^{36}Ar$: lower $^{40}Ar/^{36}Ar$ show a lower $^{4}He/^{40}Ar^{*}$. This interpretation is consistent with the schematic extraction model suggested by Pineau and Javoy (1994) based on carbon isotope variation. On the other hand, Burnard (2001) also reported an internal variation of $^{4}He/^{40}Ar^{*}$ within a single MORB and the variation was interpreted as a result of degassing owing to low $^{4}He/^{40}Ar^{*}$ ratios associated with the high $^{40}Ar/^{36}Ar$. Hence, this issue remains unsolved.

In Fig. 9, all results are plotted on the $^{40}Ar/^{36}Ar$–$1/^{36}Ar$ diagram as total values. It is remarkable that except for a few cases all the samples form a rough linear trend, suggesting a simple two-endmember mixing. On this diagram, if degassing occurs under partition equilibrium between the melt and the gaseous phase, the $^{40}Ar/^{36}Ar$ remains constant and only the Ar amount decreases. Even if degassing causes mass fractionation, when the ^{36}Ar decreases to 10% of the initial amount, the $^{40}Ar/^{36}Ar$ becomes 11% higher than the initial values (e.g. Kaneoka, 1994). For example, the "inner" group of Series 1 indicates the result of some gas-loss processes. Either degassing or the existence of an alternative magmatic endmember could explain DR1A1 "clear". In order to discuss this issue, further studies with more sampling sites at different localities are required.

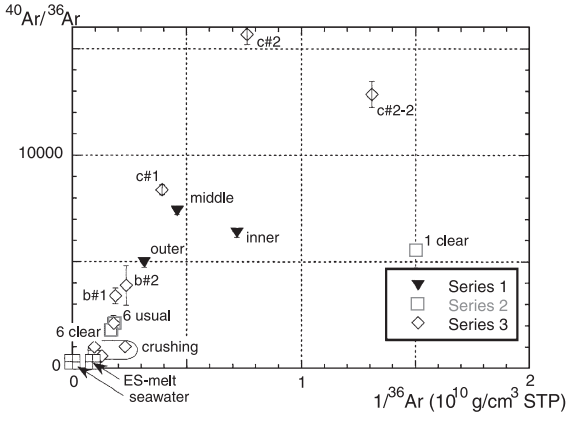

Fig. 9. Relation between the $1/^{36}Ar$ and the $^{40}Ar/^{36}Ar$, where binary mixing is expressed as a linear trend between the two endmembers. Total values are plotted in this figure. The results of crushing experiments of Series 3 are enclosed by a frame. Values of deep seawater and ES-melt are also shown.

Ballentine and Barfod (2000) argued that the atmospheric contamination in laboratory treatment could be the origin of unfractionated atmospheric component. This might also apply to this study as indicated in Fig. 9. However, the air and the ES-melt frequently show similar elemental ratios in various diagrams making it difficult to discriminate unfractionated air and ES-melt as a contaminant. In Fig. 8b, all results are plotted on the $^{132}Xe/^{22}Ne$–$^{36}Ar/^{22}Ne$ diagram as the total values of stepwise heating. The data are rather scattered because of a significant error with regard to the ^{22}Ne amount propagated from $^{20}Ne/^{22}Ne$ (ca. 20% or more). Although the data for the most samples are plotted to the left of the air–seawater mixing line with lower $^{36}Ar/^{22}Ne$ and higher $^{132}Xe/^{22}Ne$ values, the data by the crushing experiments are plotted close to but slightly below the mixing line. Aliquots from some individual samples show a rough linear trend in the heating experiment and converge at the ES-melt, so that neither unfractionated air nor seawater can affect them. This tendency of heating experiments is also observed in the $^{132}Xe/^{22}Ne$–$^{84}Kr/^{22}Ne$ diagram (not shown), which strongly suggests that the atmospheric component in the submarine sample is derived from equilibration with seawater. Variations in Fig. 9 could also be interpreted as a result of contamination by ES-melt, because the difference with seawater is small.

Here we select and plot both data by crushing and corresponding heating extractions in Fig. 8c. To simplify the figure, samples of DR1A1 Series 2 are not plotted. Crushing data are interpreted as a mixture of seawater and air, or ES-melt plotted as an extrapolated point further from the air. On the contrary,

heating data indicate a trend originating from ES-melt similar to Series 1. Although "usual" sample of DR6A1 shows much closer values to that of ES-melt compared to heating ones as in the case of "inner" group of Series 1, they were also significantly affected by seawater and/or unfractionated air. This tendency supports above mentioned hypothesis that the larger vesicles entrain seawater-derived noble gases at least in the present study.

The origin of the contamination in the 1500 °C fraction remains unclear, especially for DR6A1 "clear" and DR25A1c#1. In these samples, heavier noble gases were mostly extracted at 1500 °C, but radiogenic components were not. One possible explanation is that the atmospheric component is contained in plagioclase phenocrysts which are abundant in these samples than others. Natland (1991) argued that there were not so many phenocrysts which were directly crystallized from the erupted magma and most crystals were "xenocrysts" (Fig. 10). If such xenocrysts were derived from surrounding rocks of the magma vent affected by hydrothermal circulation, they might contain atmospheric noble gases. The $^{20}Ne/^{22}Ne$ ratio also supports this hypothesis at least for this study. On the other hand, Sarda et al. (1988) reported different case of plagioclase phyric sample that the highest $^{40}Ar/^{36}Ar$ and magmatic Ne were observed at the fusion temperature as an effect of plagioclase phenocrysts. Hence, this issue should be further investigated to specify the cause which makes such a variation in different cases.

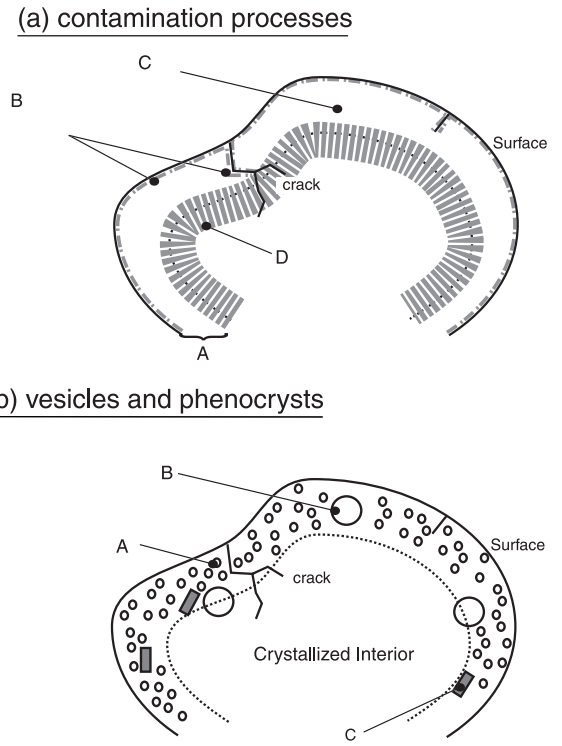

Fig. 10. Schematic drawing of (a) interpretation of contamination process in the sample of Series 1 experiment and (b) relationship of the $^{4}He/^{40}Ar^{*}$ and $^{40}Ar/^{36}Ar$ with the vesicle size within an ideal pillow fragment. In upper plate, A: Glassy layer, typically a few millimeters in thickness. B: Zone hydrated and equilibrated with seawater, typically 10 μm in thickness. C: Least contaminated zone. D: Gas-loss zone equilibrated with seawater. In lower plate, A: small vesicles which contains much He with high $^{4}He/^{40}Ar^{*}$ and $^{40}Ar/^{36}Ar$. B: large vesicles which contains less He with low $^{4}He/^{40}Ar^{*}$ and $^{40}Ar/^{36}Ar$. C: Xenocryst with low $^{40}Ar/^{36}Ar$ or phenocryst with high $^{40}Ar/^{36}Ar$.

6. Conclusions

In this study, we have examined the relationship between noble gas signatures and textures of glassy matrices for submarine glassy samples and obtained the following conclusions.

(1) The devitrified and/or color changed regions related to the "outer" zone of the sample are significantly affected by the atmospheric component, indicated by an almost atmospheric $^{40}Ar/^{36}Ar$ and $^{20}Ne/^{22}Ne$ in the 400 °C fraction.
(2) The homogeneous part assessed as the "middle" part of the glassy zone mostly retains the magmatic noble gas component: it is characterized by the most abundant He and the highest $^{40}Ar/^{36}Ar$ except for low temperature fractions. Relatively low values and small deviation of the refractive indices also support the homogeneity of samples under consideration.
(3) The transition "inner" part of glassy rind adjacent to the crystallized interior including quenched microcrystals has lost the magma-derived component. This part was contaminated by components equilibrated with seawater or derived from kinetic processes: decrease of the total gas amount except Ne which shows the lower $^{20}Ne/^{22}Ne$ compared to the others.

(4) To obtain the primary noble gas signatures of a magma from submarine glassy samples, it is suggested to select homogeneous ''clear'' glasses by excluding both color-changed and/or devitrified weathering parts and quenched microcrystals.
(5) The refractive index parameter, especially together with its deviation, helps to evaluate the homogeneity of the samples.
(6) Samples which contain large vesicles might show a low $^{40}Ar/^{36}Ar$ and a low $^{4}He/^{40}Ar^{*}$.
(7) The investigation of elemental ratios show that a component generated by interaction with seawater is a possible contaminant with the atmospheric isotope ratios.

Acknowledgements

We express our deep gratitude to T. Fujii and S. Yamashita for providing the samples and information on them. K. Endo and his staffs also provided us with a chance to use their equipment for refractive indices analyses. We also appreciate Ph. Sarda, P. Burnard and an anonymous reviewer for their constructive comments on the early version of this paper. This study was supported by the Grant-in-Aid for Scientific Research on the JSPS Research Fellowships for Young Scientists to H.K. and by the Grant-in-Aid for Scientific Research by the Ministry of Education, Science, Sports and Culture, Japan, to I.K. (Nos. 05403001, 09440182, 12440145). **[SG]**

Appendix A. Detailed descriptions of samples

Chemical compositions analyzed with EPMA installed at the Department of Earth and Planetary Sciences, The University of Tokyo are listed in Table A1 (Yamashita, personal communication).

A.1. Sample DR1A1

Recovered at the middle point of the relatively short first segment of Central Indian Ridge (25°23′S, 69°59′E). The site is located at the western slope of a seamount within the axial volcanic zone. Fresh pillows and thin sheet flows with glassy rinds of ca. 100 kg in weight were recovered. The sample is a moderately evolved aphyric tholeiitic basalt and has tiny Mn spots on the surface.

A.2. Sample DR3A1

Recovered at the northern edge of the same segment as DR1A1 (25°14′S, 69°55′E). The site is located at the flank of a seamount within the axial volcanic zone. Pillows and sheet flows with glassy rinds of more than 100 kg in weight were recovered. The sample is a moderately evolved and sparsely phyric tholeiitic basalt covered with thin Mn spots on top.

A.3. Sample DR6A1

Recovered at the middle point of the well-developed and relatively long first segment of Southeast Indian Ridge (25°48′S, 70°13′E). The site is located at the top of a seamount within the axial volcanic zone. A few kilograms of fresh glassy pieces were recovered. The sample is moderately evolved and moderately plagioclase phyric tholeiitic basalt.

A.4. Sample DR25A1

Recovered at the triple junction (25°35′S, 70°03′E). The site is located at the inner wall of the axial deep in one of the miniature segments. A few kilograms of fresh hollowed pillows with glassy rinds were recovered. The sample has a thick glassy rind of

Table A1
Chemical composition of samples

	SiO_2 (wt.%)	TiO_2	Al_2O_3	FeO*	MnO	MgO	CaO	Na_2O	K_2O	Cr_2O_3	NiO	Total
DR1A1	51.01	1.39	15.87	8.25	0.14	7.92	11.24	2.96	0.18	0.08	0.01	99.09
DR3A1	50.47	1.31	15.38	8.77	0.17	8.08	11.25	2.74	0.07	0.04	0.01	98.35
DR6A1	50.11	1.27	15.66	8.75	0.17	8.05	11.21	3.13	0.08	0.06	0.01	98.53
DR25A1	50.48	1.34	14.94	8.84	0.14	7.86	11.40	2.79	0.08	0.05	0.06	97.98

ca. 1 cm in thickness and some Pele's tears and brownish rust on the top surface. Its bottom is covered with thin Mn-coating. It is a moderately evolved and aphyric tholeiitic basalt.

Appendix B. Estimation of hydration and oxidization using refractivity

The refractive index is a sensitive parameter of the physicochemical condition of glassy materials. In subaerial tephra glass studies, refractive indices are regarded as an indicator of hydration (e.g. Steen-McIntyre, 1975) and are used for the classification of volcanic rocks or source-volcano of tephra (e.g. Church and Johnson, 1980). This parameter is closely related to the chemical composition as follows (Danhara, 1991):

$$\frac{n-1}{\rho} = K \qquad (A-1)$$

n: refractive index of a sample; ρ: density of a sample; K: specific refractivity expressed as:

$$K = \sum_{i=1}^{n} p_i k_i \qquad (A-2)$$

p_i: molar or weight fraction of the i-th oxides; k_i: specific refractivity or refractivity coefficients of the i-th oxides. Here, K of natural silicate glasses typically ranges from 0.2 to 0.22 (Danhara, 1991).

In this study, pairs of specific refractivities and molar fractions were applied to the calculation. Most oxides have close values of k around 0.2, except for H_2O, Fe_2O_3 and TiO_2; their values of k are 0.340, 0.317 and 0.398, respectively (Jaffe, 1996). Because of the less sensitive signature of K against ρ, it mainly depends on variation of p of large-k oxides. For calculation, glass densities were assumed as 2.5, then the difference of K (hereafter ΔK) becomes 0.0025: K of "usual" and "clear" are 0.2185 and 0.2160, respectively. By dividing K with k of oxides, the molar fraction (p) of oxide is obtained. In the case of the calculation of water addition, ΔK is divided by 0.340 as k_{water}, and then 8.2×10^{-3} of p_{water} is obtained as molar number of water within 1 mol sample. This corresponds to 0.23 wt.% of water. In the calculation of oxidation of Fe, ΔK is divided by the difference of k between Fe^{2+} and Fe^{3+}, 0.129 as molar number of oxidized Fe^{2+}. TiO_2 was not calculated because of its high resistance against alteration as the nature of High Field Strength Element.

References

Bach, W., Niedermann, S., 1998. Atmospheric noble gases in volcanic glasses from the southern Lau Basin: origin from the subducting slab? Earth Planet. Sci. Lett. 160, 297–309.

Ballentine, C.J., Barfod, D.N., 2000. The origin of air-like noble gases in MORB and OIB. Earth Planet. Sci. Lett. 180, 39–48.

Burnard, P., 2001. Correction for volatile fractionation in ascending magmas: noble gas abundances in primary mantle melts. Geochim. Cosmochim. Acta 65, 2605–2614.

Burnard, P., Graham, D., Turner, G., 1997. Vesicle-specific noble gas analyses of "Popping rock": implications for primordial noble gases in Earth. Science 276, 568–571.

Carroll, M.R., Webster, J.D., 1994. Solubilities of sulfur, noble gases, nitrogen, chlorine, and fluorine in magmas. In: Carroll, M.R., Holloway, J.R. (Eds.), Volatiles in Magmas. Mineral. Soc. Am., Washington, DC, pp. 231–279.

Christie, D.M., Carmichael, I.S.E., Langmuir, C.H., 1986. Oxidation states of mid-ocean ridge basalt glasses. Earth Planet. Sci. Lett. 79, 397–411.

Church, B.N., Johnson, W.M., 1980. Calculation of the refractive index of silicate glasses from chemical composition. Geol. Soc. Amer. Bull. 91, 619–625.

Danhara, T., 1991. Refractive index measurement with RIMS and its application (in Japanese). Monthly Chikyu 13, 193–200.

Danhara, T., Yamashita, T., Iwano, H., Kasuya, M., 1992. An improved system for measuring refractive index using the thermal immersion method. Quat. Int. 13/14, 89–91.

Fujii, T., Yamashita, S., Ishii, T., Tainosho, Y., Langmuir, C.H., Nakada, S., Matsumoto, S., Harada, Y., Takahashi, N., Hirose, K., 1995. Petrological sampling at the Rodriguez Triple Junction in the Indian Ocean. In: Tamaki, K., Fujimoto, H. (Eds.), Preliminary Cruise Report R/V Hakuho-maru KH93-3 Research Cruise. Ocean Res. Inst., Univ. of Tokyo, Tokyo, pp. 68–87.

Gregg, T.K.P., Fornari, D.J., Perfit, M.R., Ian Ridley, W., Kurz, M.D., 2000. Using submarine lava pillars to record mid-ocean ridge eruption dynamics. Earth Planet. Sci. Lett. 178, 195–214.

Hanyu, T., Kaneoka, I., 1998. Open system behavior of helium in case of the HIMU source area. Geophys. Res. Lett. 25, 687–690.

Hanyu, T., Kaneoka, I., Nagao, K., 1999. Noble gas study of HIMU and EM ocean island basalts in the Polynesian region. Geochim. Cosmochim. Acta 63, 1181–1201.

Hiyagon, H., 1992. Noble gas distribution in a pillow basalt from the glassy margin to the inner crystalline part: the role of noble gas diffusion and solubility (abstract). Terra Abstr. (Suppl. Terra Nova) 4, 21.

Iwata, N., 1997. Geochronological study of the Deccan volcanism by the ^{40}Ar–^{39}Ar method. PhD thesis, Univ. of Tokyo, Japan.

Jaffe, H.W., 1996. Crystal Chemistry and Refractivity. Dover, New York.

Kaneoka, I., 1994. The effect of water on noble gas signatures of volcanic materials. In: Matsuda, J. (Ed.), Noble Gas Geochemistry and Cosmochemistry. Terra Scientific Publishing, Tokyo, pp. 205–215.

Kumagai, H., 1999. Variation of noble gas signatures controlled by tectonic conditions and magmatic processes: a case study for an area around the Rodriguez Triple Junction in the Indian Ocean. PhD thesis, Univ. of Tokyo, Japan.

Kumagai, H., Kaneoka, I., 1998. Variations of noble gas abundances and isotope ratios in a single MORB pillow. Geophys. Res. Lett. 25, 3891–3894.

Matsumoto, T., Chen, Y., Matsuda, J.-I., 2001. Concomitant occurrence of primordial and recycled noble gases in the Earth's mantle. Earth Planet. Sci. Lett. 185, 35–47.

Moreira, M., Kunz, J., Allègre, C.J., 1998. Rare gas systematics in popping rock: isotopic and elemental compositions in the upper mantle. Science 279, 1178–1181.

Natland, J., 1991. Mineralogy and crystallization of oceanic basalts. In: Floyd, P.A. (Ed.), Oceanic Basalts. Blackie and Son, Glasgow, pp. 63–93.

Ozima, M., Podosek, F.A., 2002. Noble Gas Geochemistry. Cambridge Univ. Press, Cambridge.

Patterson, D., Honda, M., McDougall, I., 1990. Atmospheric contamination: a possible source for heavy noble gases in basalts from Loihi seamount, Hawaii. Geophys. Res. Lett. 17, 705–708.

Patterson, D., Honda, M., McDougall, I., 1991. Contamination of Loihi magmas with atmosphere derived noble gases: a reply to comments by T. Staudacher, P. Sarda and C. Allègre. Geophys. Res. Lett. 18, 749–751.

Pineau, F., Javoy, M., 1994. Strong degassing at ridge crests: the behaviour of dissolved carbon and water in basalt glasses at 14°N, Mid-Atlantic Ridge. Earth Planet. Sci. Lett. 123, 179–198.

Samson, S.D., Alexander Jr., E.C., 1987. Calibration of the interlaboratory $^{40}Ar-^{39}Ar$ dating standard, MMhb-1. Chem. Geol., Isot. Geosci. Sect. 66, 27–34.

Sarda, Ph., Moreira, M., 2002. Vesiculation and vesicle loss in mid-ocean ridge basalt glasses: He, Ne, Ar elemental fractionation and pressure influence. Geochim. Cosmochim. Acta 66, 1449–1458.

Sarda, Ph., Staudacher, Th., Allègre, C.J., 1988. Neon isotopes in submarine basalts. Earth Planet. Sci. Lett. 91, 73–88.

Sarda, Ph., Moreira, M., Staudacher, Th., 1999. Argon–lead isotopic correlation in Mid-Atlantic Ridge basalts. Science 283, 666–668.

Spasennykh, M.Y., Tolstikhin, I.N., 1993. Noble gas fractionation during the degassing of melts. Geochem. J. 27, 213–217.

Staudacher, Th., Allègre, C.J., 1982. Terrestrial xenology. Earth Planet. Sci. Lett. 60, 389–406.

Staudacher, Th., Sarda, Ph., Richardson, S.H., Allègre, C.J., Sagna, I., Dmitriev, L.V., 1989. Noble gases in basalt glasses from a Mid-Atlantic Ridge topographic high at 14°N: geodynamic consequences. Earth Planet. Sci. Lett. 96, 119–133.

Staudacher, Th., Sarda, Ph., Allègre, C.J., 1991. Comments on "Atmospheric contamination: a possible source for heavy noble gases in basalts from Loihi seamount, Hawaii" by D.B. Patterson, M. Honda, and I. McDougall. Geophys. Res. Lett. 18, 745–748.

Steen-McIntyre, V., 1975. Hydration and superhydration of tephra glass—a potential tool for estimating age of Holocene and Pleistocene ash beds. In: Suggate, R.P., Cresswell, M.M. (Eds.), Quaternary Studies. Royal Society of New Zealand, Wellington, pp. 271–278.

Watson, E.B., 1994. Diffusion in volatile-bearing magmas. In: Carroll, M.R., Holloway, J.R. (Eds.), Volatiles in Magmas. Mineral. Soc. Am., Washington, DC, pp. 371–411.

Yokoyama, T., Danhara, T., Yamashita, T., 1986. A new refractometer for volcanic glass (in Japanese, with English Abstr.). Quat. Res. 25, 21–30.